frontiers in Materials

REVIEW
published: 18 October 2019
doi: 10.3389/fmats.2019.00260

Oxygen Defects and Surface Chemistry of Reducible Oxides

F. M. Pinto[1], *V. Y. Suzuki*[2], *R. C. Silva*[2] *and F. A. La Porta*[2]*

[1] *Engineering Department, Federal University of Lavras, Lavras, Brazil,* [2] *Laboratory of Nanotechnology and Computational Chemistry, Federal Technological University of Paraná, Londrina, Brazil*

The magic reducible oxides properties likely are mainly due to the presence of oxygen defects and their rich surface chemistry, which provide a rational pathway to the emergent of entirely new properties. Although significant progress has performed in the last years, it can be stated that they are not fully understood at the nanoscale level so far. This mini-review provides a comprehensive perspective on the oxygen defects and surface chemistry of reducible oxides based on materials with two-dimensional (2D) structure. Thus, in this perspective, we intend to discuss some of the main challenges and opportunities in this important field of research in materials chemistry and engineering. From a practical standpoint, chemical insights from defect-engineering may provide vital clues for improving synthetic methods and understanding fundamental nanoscale properties, driving innovation in the field of reducible oxides based on 2D structure materials.

Keywords: reducible oxides, surface chemistry, structural defects, catalysis, CeO_2 (ceria)

OPEN ACCESS

Edited by:
P. Davide Cozzoli, University of Salento, Italy

Reviewed by:
Kourosh Kalantar-zadeh, University of New South Wales, Australia
David Mora-Fonz, University College London, United Kingdom

***Correspondence:**
F. A. La Porta
felipe_laporta@yahoo.com.br; felipelaporta@utfpr.edu.br

Specialty section:
This article was submitted to Colloidal Materials and Interfaces, a section of the journal Frontiers in Materials

Received: *17 April 2019*
Accepted: *01 October 2019*
Published: *18 October 2019*

Citation:
Pinto FM, Suzuki VY, Silva RC and La Porta FA (2019) Oxygen Defects and Surface Chemistry of Reducible Oxides. Front. Mater. 6:260. doi: 10.3389/fmats.2019.00260

INTRODUCTION

Given the environmental and political problems created by the dependence on fossil fuels, combined with the likely decline in oil reserves, in particular, the search for new renewable sources of energy and chemicals has become increasingly important. To address this issue, significant efforts have been undertaken to diversify our energy sources, particularly for the transport sector, and hence point the way to find cleaner energy sources. However, alternative fuels are not available in all places, and one region may prefer ethanol, while another biodiesel, gasoline, or methanol. Most fuels require different engine technologies for efficient operation, as well. However, hydrogen can in principle be produced from various raw materials and is a by-product of the above-mentioned alternative fuels, as well as many others, i.e., providing a promising alternative and universal fuel (Holladay et al., 2009).

The conversion of larger molecules present in biodiesel or petrochemical derivatives to hydrogen involves several steps that must be well-controlled to obtain the desired product. Thus, the use of catalysts in complex and multi-step reactions is fundamental in order to aid the process (Trane et al., 2012). The process of converting complex molecules to H_2 involves separate oxidation and reduction steps. Therefore, a desirable catalyst must exhibit this duality. In addition to being very active, the catalyst must be easily produced and also exhibit high stability with a long lifespan. In this context, oxide catalysts can widely be used as promising alternatives in order to meet these demanding requirements. Before use in catalysis, reducible oxides have been extensively used in the fields of superconducting physics and spintronics because of their excellent ionic mobility at high temperatures (Barcaro and Fortunelli, 2019). According to Professor Misono: "A catalyst can be called catalytic converter only when it catalyses some reaction useful for practice and the society."

He states that, "the progress of catalysts based on mixed and reducible oxides may be the key to the advancement of catalytic technologies" (Misono, 2005). The improvement of the catalytic performance of reducible oxides has attracted significant interest from the scientific community in order to better understand their mechanisms and electronic structures at the nanoscale.

In this review, a brief discussion will be presented regarding reducible oxides based on materials having two-dimensional (2D) structure as well as their formation, migration, and dimerization of vacancies. The potential use of these advanced materials for the production of hydrogen from biomass and bio-oil as well as in the gas-water displacement reaction and the preferential oxidation of CO will also be reviewed.

WHAT ARE REDUCIBLE OXIDES?

Reducible oxides are solid state materials that are strongly affected by the reversible oxidation state of the metal. Because of the reversibility, these materials are promising for storing and releasing oxygen, as well as, for a huge variety of catalytic processes. It has been established that a reduction in the oxidation number of the metal occurs when the crystal loses an oxygen atom and forms a vacancy. In addition, it has also been observed that the reduction of particle size can, in theory, increasing the stability of the metal in their many applications (Van Santen et al., 2015). This key phenomenon is shown schematically in **Figure 1A**.

Thermodynamically, any oxide is reducible (Swartz, 2002), but oxygen vacancies are defects preferentially formed under low partial pressures of oxygen and high temperatures. Hence, the distinction between a reducible and non-reducible is typically associated with the necessary conditions for vacancy formation to occur. For reducible oxides, these conditions (e.g., temperature and pressure) are moderate and technically attainable, while the corresponding conditions necessary to form vacancies in non-reducible oxides are, in theory, more difficult to be achieved (Swartz, 2002; Schaub et al., 2003; Wahlstro et al., 2004). To illustrate these conditions, Paier et al. (2013), used a density functional theory (DFT) framework to investigate CeO_2 (111), TiO_2 (110), Al_2O_3 (0001), and MgO (001). The results of their calculations are reproduced in **Figure 1B**.

From the analysis of **Figure 1B**, it is clear that two oxide surfaces can be considered "reducible," CeO_2 (green) and TiO_2 (blue) because the conditions required for thermodynamically favorable reducibility are attainable. However, for Al_2O_3 and MgO, these conditions are quite extreme and therefore are usually considered to be non-reducible (Barcaro and Fortunelli, 2019). Hence, the necessary conditions for the emergence of complex defects have been extensively studies, where some authors have identified the formation of temperature defects (Namai et al., 2003a,b), while others have observed vacancies arising only above 400°C (Esch et al., 2005). It is likely that oxygen vacancy formation depends on many factors, including the inherent nature of the analyzed oxide, its purity, surface analysis, synthesis condition, and also doping status. It is possible to observe vacancies at ordinary room temperature with a high degree of "contaminants" favoring the vacancy-like formation. These factors will be further discussed in the following sections. Among the various reducible oxides, we are particularly interested in TiO_2, CeO_2, ZrO_2, V_2O_5, FeO_X, PrO_2, SmO_X, CoO_X, MnO_X, V_2O_5, MoO_3, and WO_3 and more complex solids, such as the $BaTiO_3$, $LaCoO_3$, and $HfSiO_X$ (Livage, 2010; Paier et al., 2013; de Castro et al., 2017).

Electronic Structure

The migration of electrons from the oxygen 2p orbital states in the valence band (VB) to the conduction band (CB) (**Figure 1C**), is only possible if the energy between them (band gap) is relatively small, on the visible and ultraviolet radiation frequency. For example, reducible oxides are usually formed by metals that contain half-filled d and f orbitals, it is additionally likely which such compounds form a mix of covalent or ionic bonds. For Ce these are the 4f orbitals; 3d orbitals for Ti and V; and 4d for Zr. In oxides considered to be non-reducible, the d and f orbitals are typically unoccupied (for example, Mg and Al), forming likely a large band gap, making the high energy intermediate and thermodynamic electron migration unfavorable (Esch et al., 2005). These modern computational methodologies, however, have inspired notable progress in the field of catalysis (Seh et al., 2017). Thus, computational catalyst design has played a growing role in developing sustainable next-generation nanoscale complex materials and is typically at the forefront of scientific study in the field of catalysis.

Where Do Vacancies Come From?

The energy requirements for the formation of vacancies in reducible oxides is relatively low compared to that of other materials and is thermodynamically favorable at high temperatures and low partial pressures of oxygen (Rasmussen et al., 2004; Esch et al., 2005; Zhou et al., 2008; Paier et al., 2013). For all cases, are expected to vacancy formation is thermodynamically more favorable at terraces and surfaces than inside the bulk oxide. In other words, the formation of surface vacancies is favored due to the greater interatomic potential (the potential between two bodies that arises due to the steric repulsion of ions) inside the oxide (Nolan et al., 2006). The coordination number of the exposed surface exposed is less than that inside the network, i.e., facilitating the formation of a considerable amount of surface defect states. Surfaces with smaller coordination numbers favor, therefore, the defect formation. Esch et al. (2005), monitored the formation of oxygen vacancies in CeO_2 (111) by scanning tunneling microscopy (STM) and the obtained images are shown in **Figure 2**.

From these results, the presence of subsurface vacancies (blue triangles) and "dumbbell" type or trimers (red triangles) vacancies can in principle be observed. At the bottom of **Figure 2** there is a schematic of the ordering of the oxygen and cerium atoms in each type of vacancy. The formation of vacancies occurs in the subsurface (second layer) because those metal atoms are reduced and the outermost layer is composed primarily of oxygen atoms. However, when a vacancy is typically formed, it exposes two Ce^{3+} atoms and one Ce^{4+} atom that is smaller than Ce^{3+}. Because of the size, the total power of the network

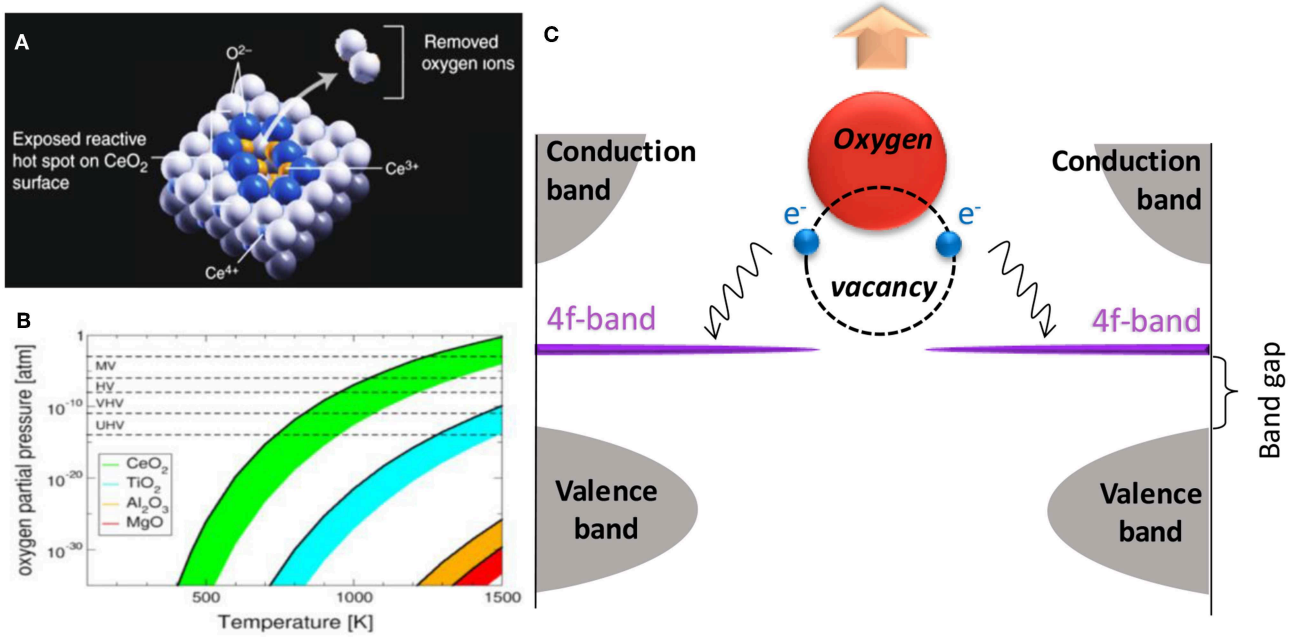

FIGURE 1 | (A) Illustration of vacancy formation on the surface of ceria; **(B)** Phase diagram of the transition curves of the crystalline structure in the presence of O_2 obtained by DFT (MV, medium vacuum; HV, high vacuum; VHV, very high vacuum; and UHV, ultra-high vacuum) and **(C)** Schematic of vacancy formation and its impact on the electronic levels of a reducible oxide (adapted from Esch et al., 2005; Sun et al., 2012; Paier et al., 2013).

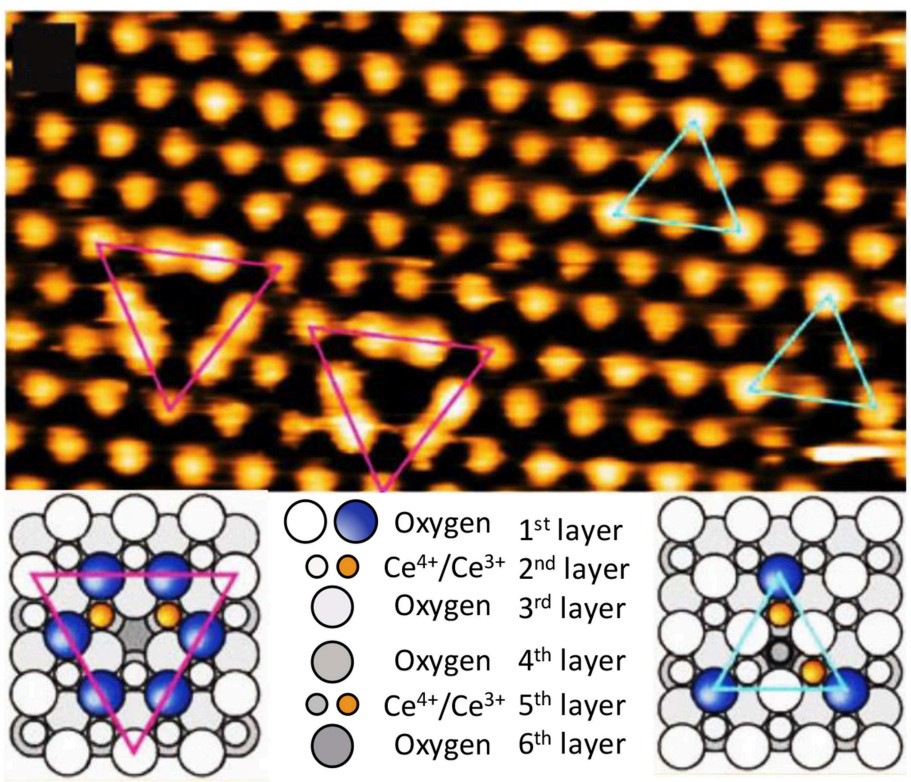

FIGURE 2 | STM images of oxygen in the CeO_2 facet (111) (adapted from Esch et al., 2005).

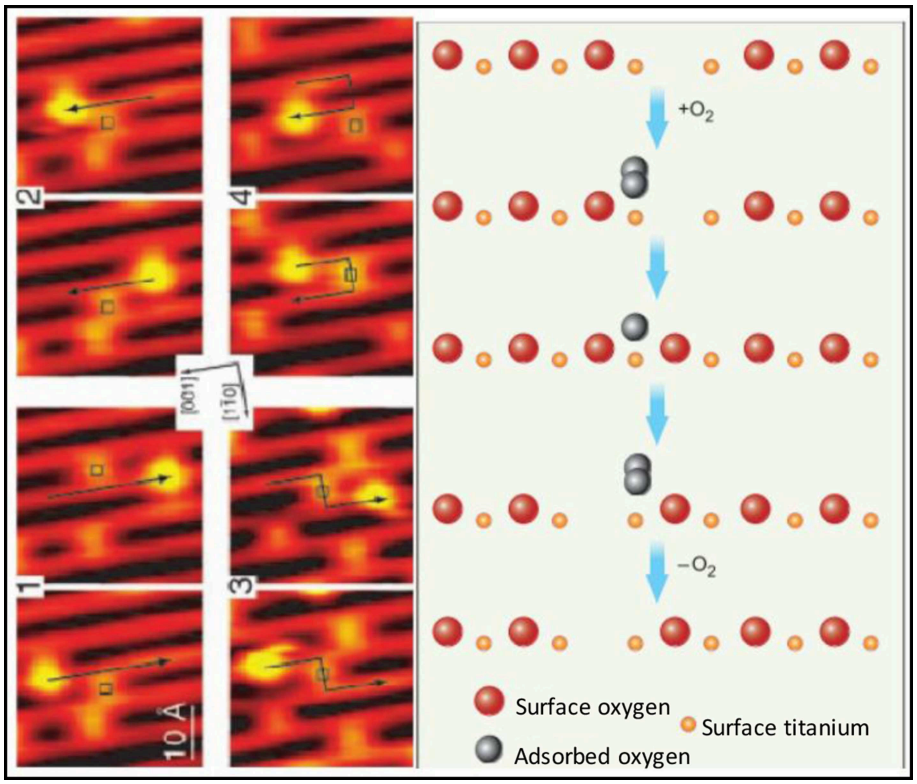

FIGURE 3 | Mobility of oxygen vacancies on the surface of TiO_2. STM images (left) and schematic diagram (right) (adapted from Campbell, 2003; Schaub et al., 2003). In the left images, each number symbolizes the microscopy of a region different. Each number shows two microscopy images, the first before the movement and the second after the move.

increases. Once formed, a wave becomes a positive center that attracts electronegative species like O_2. Generally, when they are attracted, the defect is undone and by chemisorption the O_2 is added to the surface. This chemical adsorption and migration of the defect states on the surface of TiO_2 are shown in **Figure 3**.

Another phenomenon responsible for causing the formation of vacancies is the term entropic stabilization will appear for surfaces with a large number of voids, usually obtained by removing part of the ions at a polar terminus to cause the layer to be charged is zero. In general, the surfaces of reducible oxides are highly disordered at nanoscale (Capdevila-Cortada and López, 2017; Mora-Fonz et al., 2017).

After adsorption on the surface, one atom in the oxygen molecule can recombine (and again form O_2) with the same oxygen atom or with a neighboring oxygen atom. Thus, in this perspective, the vacancies become mobile and can occupy any spot on the surface of the network, since the energy at any point on the surface (assuming a clean surface) is identical (Campbell, 2003; Schaub et al., 2003; Esch et al., 2005). After acquiring a certain mobility, vacancies tend to occupy low energy spaces, i.e., regions where the total energy of the network is minimal. It was previously mentioned that during the formation of a vacancy, two atoms of the metal are exposed and one metal atom is in its initial oxidation state. When dimerizing, these clusters of vacancies expose only reduced metal atoms without distortions in the crystalline lattice and are, therefore, thermodynamically more favorable. The phenomenon of vacancy dimerization and exposure of reduced metal atoms in these dimers is shown in **Figure 4**.

In an interesting study, Esch et al. (2005), used STM at different times for CeO_2 samples exposed to a temperature of 900°C under vacuum and the images are shown in **Figure 5**. From **Figure 5**, it is clear that with increasing exposure time to 900°C conditions, an increased number of vacancies was observed, especially in the form of dimers. Over time, in particular, the number of vacancies stabilized and the structure equilibrated. Bryant et al. (2011) showed that the surfaces of $PrSr_2Mn_2O_7$ contain vacancies and peaks formed by the adsorption of oxygen. Hence, the adsorbed oxygen atoms are called adatoms (ad = adsorbed and atom = atom). An illustrative scheme of this scenario is shown in **Figure 6A**.

Bryant et al. (2011) also performed STM in order to monitor the vacancy behavior, which are shown in **Figures 6B,C**.

In **Figures 6B,C** the recombination between a vacancy and an adatom to form a "flat" site on the $PrSr_2Mn_2O_7$ is shown. This recombination demonstrates that reintroducing oxygen to the reducible oxide structure is possible, as well as, conferring a cyclical capacity to undergo reduction (vacancy formation) and return to the original state (reincorporation of oxygen into the structure). Applications of the cyclic capacities of these materials

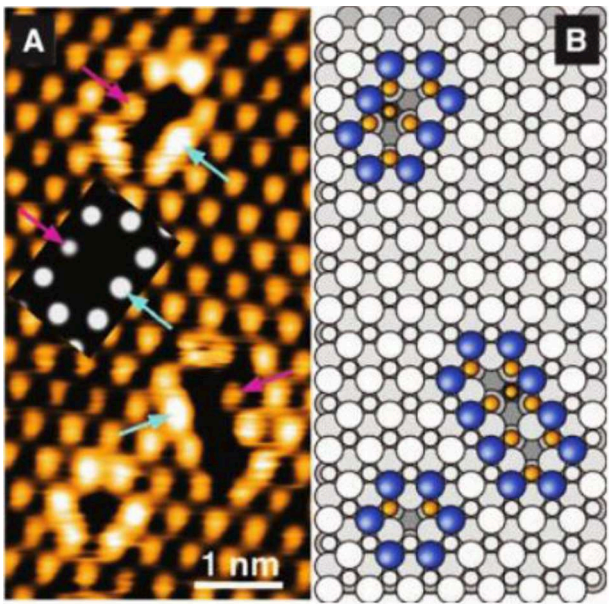

FIGURE 4 | Dimerization of the oxygen vacancies in the CeO_2 facet (111) **(A)** STM image **(B)** Corresponding structural model (Adapted from Esch et al., 2005).

will be further discussed below. Oxides, in addition to oxygen vacancies, may also contain interfacial defects, which also called planar or line defects, in their crystalline structure (Callister and Rethwisch, 2012). For instance, such imperfections include external surfaces, grain contours, phase contours, edge contours, and stacking faults. Notably, considering the grain boundary has different crystallographic orientations and are usually contours that have naturally two dimensions, which also separate the materials. So there is an interfacial or grain boundary energy similar to the surface energy (which depends on the exposed face and the growth direction). Hence, the magnitude of this energy is due to the degree of disorientation, being more significant for the high angle contours, while the grain boundaries are, in theory, more reactive (Callister and Rethwisch, 2012). Also, naturally the impurities atoms incorporated into the host material often segregate in the contours (i.e., due to their higher energy levels). In this case, the interfacial energy is, in turn, that lower in materials with larger or coarser grains, precisely because of the grain boundaries. However, in this perspective, despite the disordered disarray of the atoms and the lack of a regular bond along the contours of the grains, a polycrystalline material is very resistant, likely since cohesive forces are present in and through the contours (Callister and Rethwisch, 2012).

However, many recent studies have shown that advanced materials containing high-density grain boundary defects can give rise to new and unique functionality for a huge diversity of emergent applications (Guo and Waser, 2006; Lee et al., 2012). For instance, in a study conducted by Feng et al. (2016), provide clues that the amount of oxygen vacancy presents in CeO_2 materials as-prepared are highly dependent on the structure of grain boundary defects, and hence are key in order to elucidated their catalytic nanoscale behavior.

Adding Dopants and Forming Vacancies

Aristotle's famous quote "the material behaves differently from its components" perfectly fits this subitem. Upon addition of dopants, a different metal ("impurity") is added to the reducible oxide increasing the entropy of the system by disrupting the crystal lattice and decreasing the energy required to form vacancies. In this manner, non-reducible oxides can become reducible when suitably doped. Hence, in this perspective, the primary effect of vacancy formation after the addition of a dopant to the structure is cargo conservation. For example, by adding a 3+ dopant to the structure of a network formed by atoms in the 4+ state will result in the formation of a vacancy (½ O_2 output) for every two 3+ dopant atoms added. However, is well-known that vacancy formation in doped complex oxides also depends on the size of the dopant and Coulomb interactions that are governed by the oxidation state of the dopant metal and its polarizability. Reduction of the metal is favored when the dopant added to the structure exhibits characteristics similar to those of reduced metal. When a dopant is introduced with a radius greater than that of the oxidized bulk metal, the metal will be reduced, increasing its size, reducing the distortion of the network, which minimizes the network. In parallel, the energy of vacancy formation decreases with increasing ionic radius of the dopant added, which is shown in **Figure 7A**.

From **Figure 7A**, it is clear that increasing ionic radius of the dopant affecting the overall shielding energy (energy required to form a vacancy-like). However, with increasing dopant atom size (Gd → La), in particular, the shielding energy increased. Another important factor, as shown in **Figure 7**, is the reliability of the prediction calculations of the behavior of the metal-doping alloys. Although the precision is lacking, the overall trend of the curve was followed for the calculated and empirical models. Coulomb interactions, in general, depend on the polarizability of each ion and overall polarization. Thus, stronger interactions and lower energy locations are necessary for vacancy formation. The effect of polarizability is shown in **Figure 7B**, depicting the decreasing reduction energy (vacancy formation) with increasing concentration of Th and Zr dopants. Hence, the decrease in the reduction energy upon Th doping more pronounced due to its greater ionic radius and polarizability. In addition, it is well-known that the 2D structures of ceria can be achieved by utilizing various synthetic routes available (Umar et al., 2015; Song et al., 2017; Li et al., 2018). In this context, Li et al. (2018) have reported the possible to get cerium oxide with nanoflakes forms with more active planes by doping with cobalt using the hydrothermal method as a strategy. According to these XRD results, in particular, the doped product had a cubic fluorite structure belonging to the Fm-3M group (no: 225) with a = 5.41134 Å (Morris et al., 1964). They reported that the Co-CeO_2 system have an excellent catalytic activity for the Hg^0 removal. Particularly, the Hg^0 is oxidized by active oxygen species of doped host matrix, which were associated with the oxygen defects caused in the CeO_2 lattice (Li et al., 2018). In this case, it is well-known that such species have high mobility. Optical responses has been widely applied to identify the presence of structural defects in many materials (Kripal et al., 2011; Wang et al., 2013; Liu et al., 2014). For instance, Eu(III) ions are usually

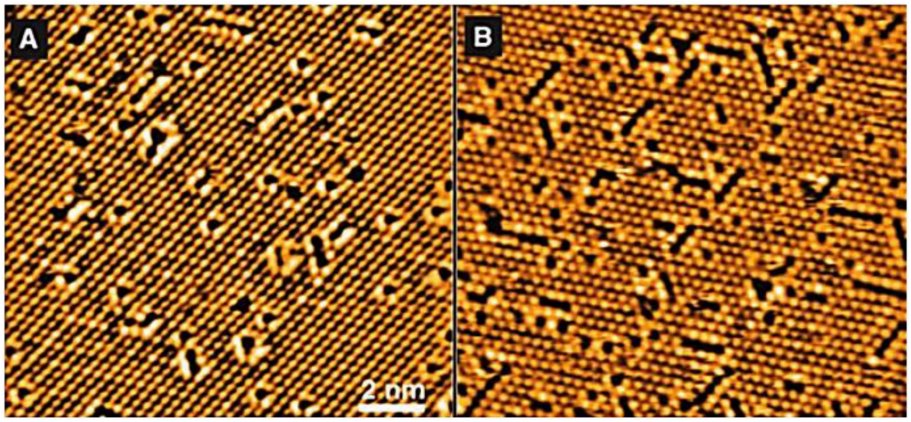

FIGURE 5 | Growth of oxygen vacancies in CeO_2 (111). **(A)** 1 min and **(B)** 5 min of exposure to 900°C (adapted from Esch et al., 2005).

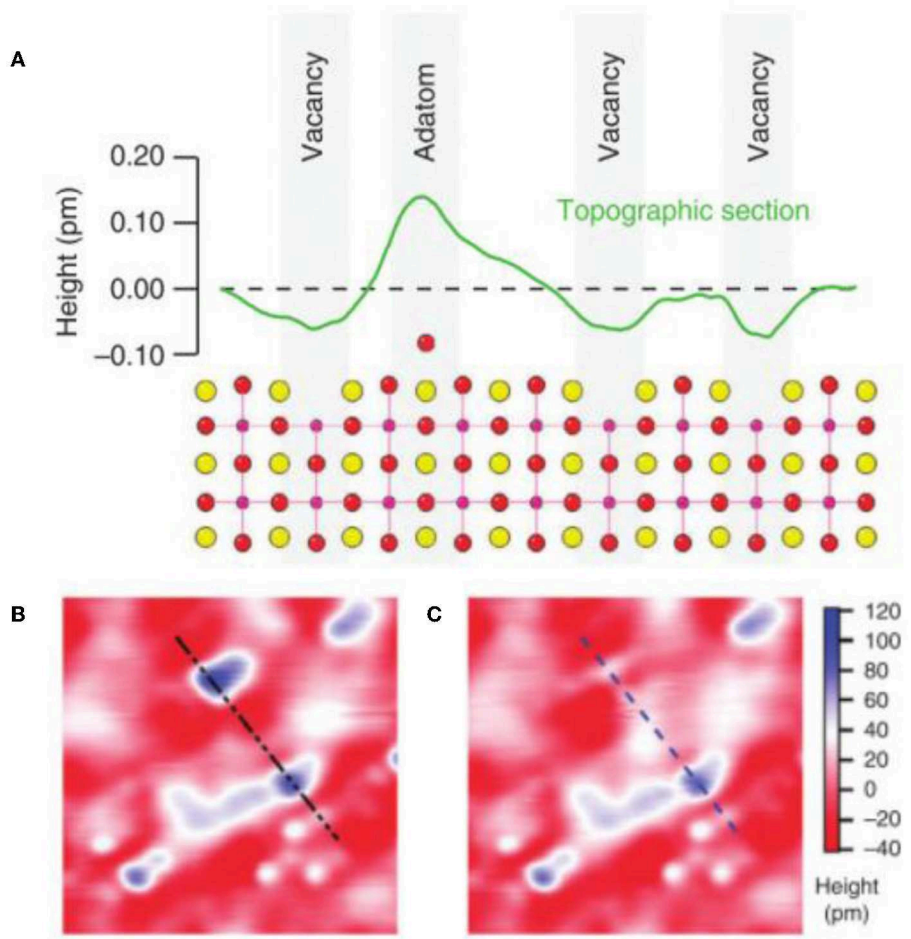

FIGURE 6 | (A) Schematic of the surface topography of a generic reducible oxide with its their respective adatomos and vacancies. **(B,C)** Microscopies (STM) separated by 1 min showing the recombination between adenomas and vacancies (adapted from Bryant et al., 2011).

used to probe the local structure of diverse materials (Montini et al., 2009; Tiseanu et al., 2014). It is reasoned that the intense $^5D_0 \rightarrow {}^7F_0$ transition of Eu(III) ions can be mainly used in this context to differentiate its preference of incorporation in bulk and the surface of the host matrix (Montini et al., 2009) as shown in **Figure 8A**. In parallel, a single well-defined UV-vis

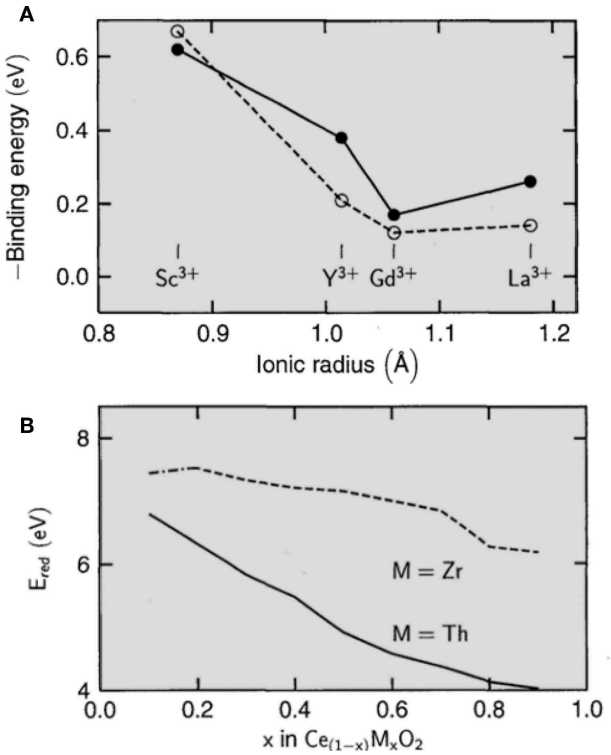

FIGURE 7 | (A) Ce^{4+}/Ce^{3+} reduction energy (calculated → solid line; experimental → dashed line) as a function of dopant composition and **(B)** Ce^{4+}/Ce^{3+} reduction energy (calculated → solid line; experimental → dashed line) as a function of dopant composition (adapted from Trovarelli and Fornasiero, 2013).

absorption peak at 344 nm was observed for the CeO_2 nanoflakes (see **Figure 8B**). From the characterization of the sample by Raman scattering it was possible to notice that the dominant peak at 464 cm^{-1} is attributed to the CeO_2 characteristic band and corresponds to the active mode F_{2g} of the CeO_2 cubic structure (see **Figure 8D**) (Lu et al., 2010; Liu et al., 2011). The other four weak Raman modes (377, 429, 550, and 593 cm^{-1}) characterize structural disorder in CeO_2 lattice (Grover et al., 2008; Araújo et al., 2012; Aškrabiać et al., 2012). In order to study the mobility of oxygen, O_2-TPD was tested for different temperatures. **Figure 8C** showed that pure CeO_2 peaks at 200–300 and 400–650°C were attributed to surface oxygen poorly bound to surface and chemically adsorbed oxygen species at vacancies, respectively (Jiang et al., 2015). When comparing to pure CeO_2, the increased chemical adsorption of O_2 between 100 and 500°C Co-CeO_2 suggested that it has a more efficient activation at its surface due to increases of oxygen vacancies (Zheng et al., 2016). As result, these structural defects are responsible for creating new intermediate levels within the band gap, which can be a more active site for many reactions. Hence, photocatalytic activity of CeO_2 nanoflakes was evaluated by the degradation of DR-23 dye under UV irradiation (Umar et al., 2015). A proposed mechanism is presented in **Figure 8E**, and is consistent with the literature (Umar et al., 2015).

Metals Supported on Oxides

The use of metals supported on reducible oxides has become increasing popular for heterogeneous catalysis development. The high catalytic conversion, cycling potential, and affordability of these catalysts has attracted significant interest from researchers in industry and academia (Rodríguez and Hrbek, 2010). Supports based on mixed oxides have been widely used for catalysis (CeO_2 and TiO_2 are particularly outstanding), due to their relatively high area, thermal stability, and their function as a carrier and catalytic promoter. The "reducible oxide + electron donor metal" system has been used often in the literature and in various forms (**Figure 9**). The interface between the oxide and metal is the most active catalytic site in these materials and is referred to as the "hot spot zone."

The electron donor metal functions as a promoter for vacancy formation and the other side the oxide can provide electrons (opposite direction of the reduction) to the metal. This "oxide + metal" system is active for oxidation and redox reactions (Vayssilov et al., 2011). An example of vacancy formation in reducible oxides with the addition of electron donors is shown in **Figure 10**. Upon addition of Cu to CeO_2, the peak intensity at about 533 eV decreased compared to the peak at 530.5 eV. Hence, the component with the O1s electrons trapped is commonly attributed to the presence of vacancies (Hardacre et al., 1995). Thus, the addition of donor metals favors vacancy formation through electron donation. On the other hand, the interaction between the metal and oxide depends on the size of the structures. These materials have a larger area per unit mass and vacancy formation occurs preferentially on the surface, causing an energy reduction. In addition to the high surface area, the nanostructured materials promote greater interaction between the electron donor metals, dopants, and reducible oxide, forming additional "hot spot zones" (Migani et al., 2010; Vayssilov et al., 2011).

Interaction With Oxygen

Understanding the interaction mechanism of oxygen molecules with reducible oxide surfaces is crucial for understanding of oxide catalysts. The formed vacancies interact with O_2 molecules (see **Figure 11**), forming peroxo [MOOM] species on the surface, which are extremely reactive and strong oxidants (Paier et al., 2013).

Due to the increase in bonding distances relative to O_2 and also the corresponding displacement of the O-O, superoxo, and peroxo stretching frequency, surface species which can be experimentally identified from the vibrational (infrared or Raman) spectroscopy. Hence, the adsorption energy of the different species of oxygen by the surface of the metal (as shown in **Figure 11**) alters the dynamics of oxygen donation and its reincorporation, with impacts on the reactional rate for each material (Paier et al., 2013).

Eletrochemical Potencial Use

In the application of photovoltaic solar energy, as it is widely abundant, such devices may in principle provide more sustainable clean, green energy without toxic or dangerous gases (Nunes et al., 2018). The designed materials for these

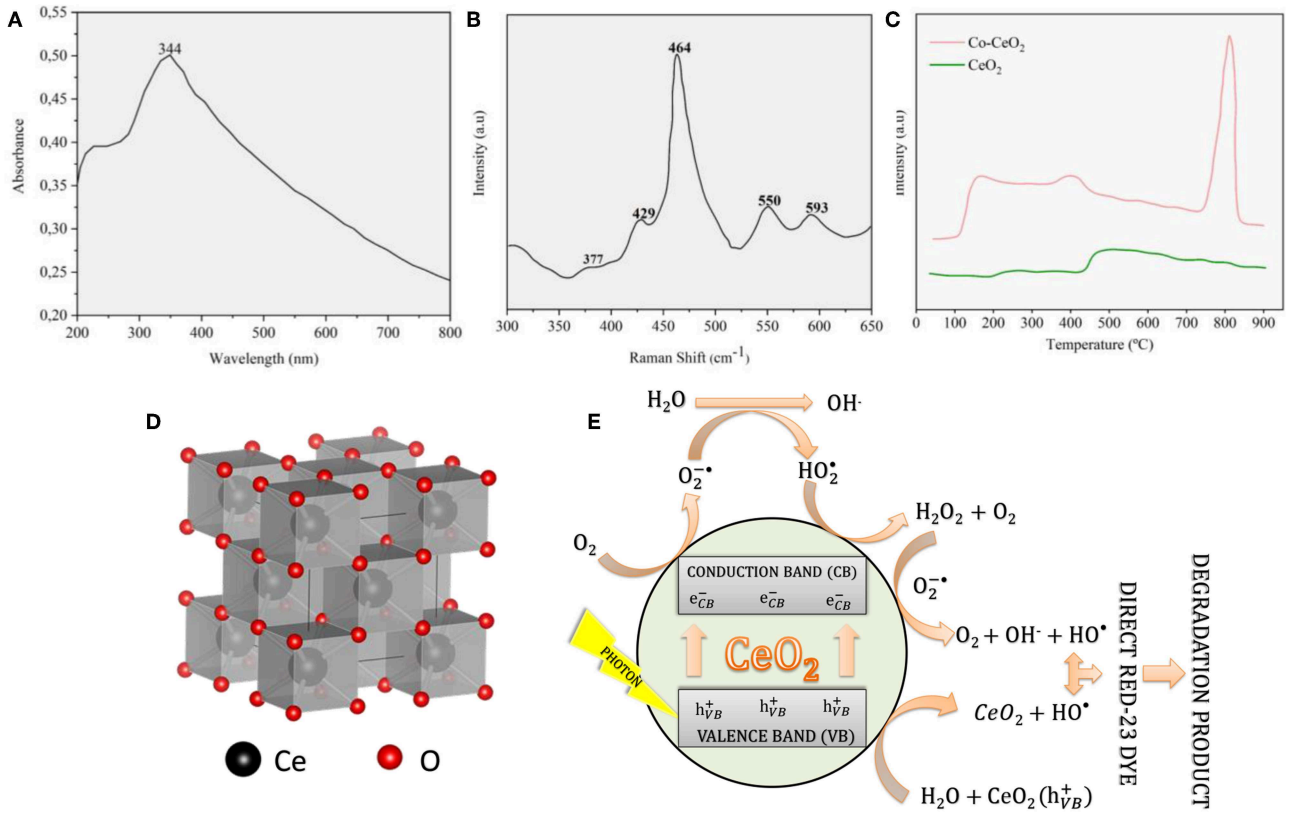

FIGURE 8 | (A) UV–Vis spectrum UV-Vis spectrum of CeO_2 nanoflakes, **(B)** Raman-scattering spectrum of prepared CeO_2 nanoflakes, **(C)** O_2-TPD profiles of pure CeO_2 and Co-CeO_2 **(D)** CeO_2 unit cell and **(E)** Pictorial representation of degradation mechanism for the photocatalytic degradation of DR-23 under UV-light irradiation (adapted from Umar et al., 2015; Li et al., 2018).

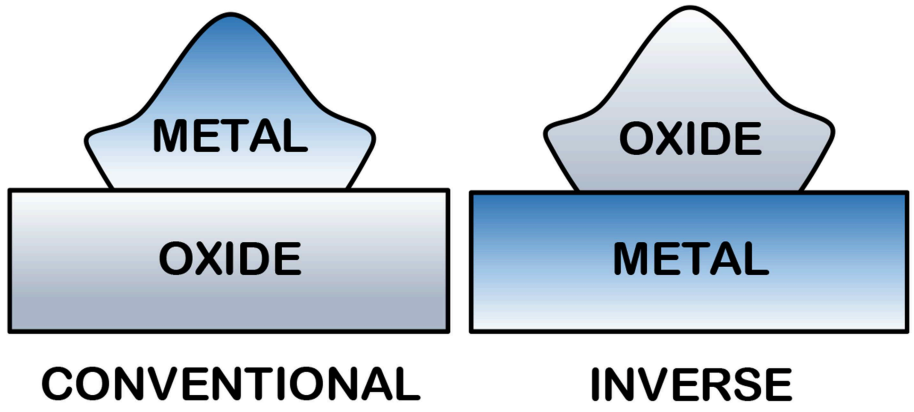

FIGURE 9 | Structure of the conventional and inverted catalysts (adapted Rodriguez et al., 2009; Rodríguez and Hrbek, 2010).

applications have increased a lot in recent years, which has transformed the total cost of this technology, likely is due to the fast increase in efficiency as well as the simplicity of fabrication of these devices. For instance, photovoltaic devices based on silicon can be considered, currently, as the main photovoltaic material used today, prevailing the photovoltaic market with a high-power conversion efficiency (PCE) up to 27.6%, however, it has high production costs (Glunz et al., 2012; National Renewable Energy Laboratory, 2019; Velilla et al., 2019). Fine-film solar cells based on perovskite-related materials are also under intense investigation, however, where these devices exhibit PCEs normally in the range of 10 to 25%. More recently,

several strategies have widely been adopted to the development of the next generation of photovoltaic devices, especially based on emerging materials (Protesescu et al., 2015; Brenner et al., 2016; Manser et al., 2016; Saliba et al., 2016). These novel emerging materials are chemically and thermally stables with incredible potential for many applications and, in some cases, can widely be compatible with a huge variety of low-cost manufacturing (Masi et al., 2018; Nunes et al., 2018; Fernandes et al., 2019; Ramirez et al., 2019). Such emerging materials, however, have its chemistry still very little explored, which may in principle be an option interesting for the appearance of many technologies.

Eventually, when considered the evolution of solar cells with the most remarkable achievements also includes dye-sensitized solar cells (DSSCs), which have played a prominent role in the past but remain very important for photovoltaic technology (O'Regan and Gratzel, 1991; Wang et al., 2006; Gong et al., 2017). In the DSSCs, particularly, the mesoporous metal oxide mainly the basis of TiO_2 with PEC < 8% (Sharma et al., 2017). However, many other oxides may also be used for applications in DSSCs are integrated into devices anchored to the dye is placed between two glass conductive plates in the presence of an electrolyte, which is generally a redox system (Polman et al., 2016; Sharma et al., 2017; da Fonseca et al., 2018). Fundamentally, by drawing attention to DSSC application, when dye molecules (also known as photosensitizers) capture the photons of sunlight. Consequently, the photoelectrons move directly from the LUMO (lowest unoccupied molecular orbital), which is the excited state of the dye (a liquid redox electrolyte, usually I^-/I^{3-} non-aqueous solution), to the CB of the semiconductor material as electron selective contact and therefore diffuse to the electrode conductor (da Fonseca et al., 2018; Nunes et al., 2018). Hence, the ionized dye molecules are, in turn, reduced by the reducible oxide charge on the electrolyte. Additionally, the dye is electrochemically regenerated in this process (Nunes et al., 2018).

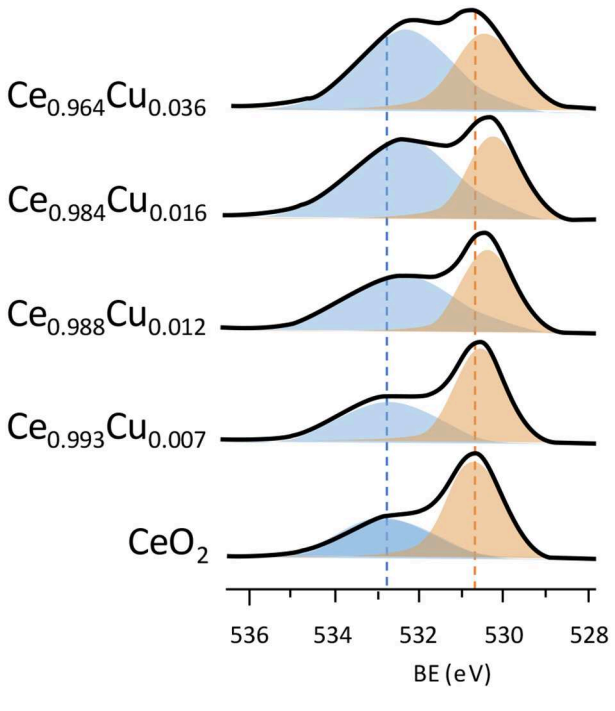

FIGURE 10 | Spectrum of XPS O1s and the effect of copper doping on ceria (adapted from Aranda et al., 2012).

REDUCING OXIDES APPLIED TO CATALYSIS

The huge versatility of oxide materials allows a wide range of technological applications, including catalysis, sensors, electrochemistry, energy storage, photochemical energy conversion, and fuel cells (Seh et al., 2017). When discussing the use of reducible oxides in catalysis, we should mention their use in oxygen storage, emissions control in diesel engines, hydrocarbon oxidation, three-way catalysts, and hydrogen production. Hydrogen production can be achieved using several sources including biomass and bio-oil, and via reactions such as gas-water displacement (water gas shift) and preferential oxidation of CO (Prox) (Trane et al., 2012).

Hydrogen Production From Biomass

Biomass is organic matter (non-fossil) of animal or vegetable origin, capable of being used as a source of energy. Common examples include straw, bagasse, rice husk, sawdust, wood chips, briquettes, and vegetable oils (biodiesel) (Barandas, 2009). Biomass was the first energy source used by mankind and its use may reduce worldwide dependence on oil. Biomass can be obtained from agricultural, industrial, and household

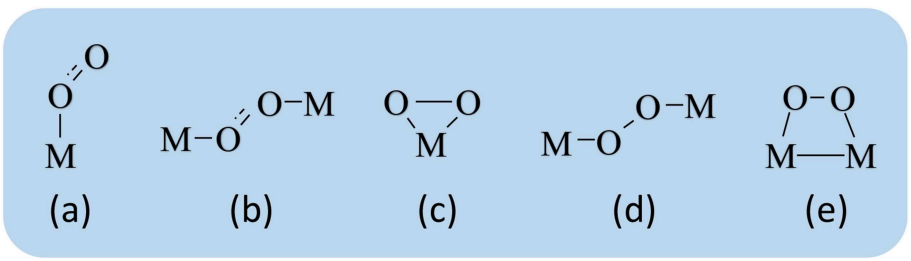

FIGURE 11 | The two types of bonding on the surface: **(a)** superoxo-η1, **(b)** superoxo-μ, **(c)** η2-peroxo, **(d)** μ-peroxo, and **(e)** trapezoid-peroxo (adapted from Wagnerová and Lang, 2011).

waste in many forms. The direct use of biomass as an energy source is unfavorable for biomasses with low calorific value. Therefore, reactions involving the H_2 and CO (called synthesis gas) have long been developed (de Lasa et al., 2011). Reactions involving biomass are usually performed by the gasification of its components through heating, which promotes the formation of a gaseous phase consisting of H_2, CO, CO_2, CH_4, tar (benzene and other aromatic compounds), water vapor, solid wastes (char), and liquids (bio-oil). The first catalysts used (and perhaps the most commonly used to date) are based on materials such as Al_2O_3, dolomite ($CaMg(CO_3)_2$), olivine ($(Mg, Fe)_2SiO_4$), and alkali metal oxides. The complexity of these reactions and rapid deactivation caused by the high carbon concentration result in a short service life for these catalysts (de Lasa et al., 2011; Trane et al., 2012). The complex reactions with high levels of carbon and formation of coke involve both reduction and oxidation steps, and the reducible oxides have been suggested as viable alternative catalysts. According to Łamacz et al. (2011), reducible oxides decompose biomass components using their vacancies, but the addition of metal donors increases the production of H_2 and CO. The authors proposed that the association between reducible oxides and electron donating metals (such as Ni, Au, Pt, and Pd) are the most promising systems for these reactions. de Lasa et al. (2011), reviewed the use of various supports (a-Al_2O_3, γ-Al_2O_3, SiO_2, MgO, CeO_2, and TiO_2) for steam reforming of biomass with Ni as the supported metal. Cerium and titanium oxides showed similar conversion efficiency during the initial cycles but deposited only smaller amount of coke (carbon deposits) on the surface. The vacancies promoted greater interaction with oxygen and promoted the oxidation of carbon deposits (de Lasa et al., 2011). Thus, the oxide carriers exhibited better performance over many cycles and are more viable for long-term use.

Production of Hydrogen From Bio-Oil

As previously mentioned, the process of biomass gasification generates gaseous, liquid, and solid products. The liquid gasification product is dark brown and referred to as bio-oil. Bio-oil consists of a complex mixture of organic compounds and small inorganic fractions. To illustrate the composition of the bio-oil, **Table 1** lists the main components and their contents.

Table 1 shows that bio-oil mainly contains water and lignin. However, the presence of aldehydes, acids carboxylic acids, alcohols, and ketones account for 45% of the bio-oil. Thus, most studies of bio-oil reforming use the aqueous fraction of the bio-oil, containing acetic acid (Basagiannis and Verykios, 2006, 2007; Vagia and Lemonidou, 2008), acetol (Barandas et al., 2011; Dubey and Vaidya, 2012), and ethanol (Song et al., 2010; Ávila-neto et al., 2012; Soykal et al., 2012). However, a major challenge for reforming bio-oil is related to the catalysts that require high activity, selectivity for H_2, and high stability. The diversity of reactions required for the conversion of oxygen compounds present in the bio-oil is shown in **Figure 12**.

Figure 12 shows the number of steps (dehydrations, dehydrogenations, hydrogenations, as well as CC and CO bond breakage) involved in the conversion of complex molecules to H_2, CO, and CO_2. For biomass reforming, catalysts based on reducing oxides are quite promising, given the number and complexity of the produced phases. These steps described in **Figure 10** involve donor and electron acceptor sites, and the mobility of these electrons as well as the reversibility of oxygen adsorption on the surface favor these reactional steps, increasing the reaction rates and minimizing the deactivation of the catalysts by carbon deposition (Cortright et al., 2002).

TABLE 1 | Chemical composition of bio-oil.

Componentes	Weight (%)*
Water	20–30
Lignin fragments: Insoluble pyrolytic lignin	15–20
Aldehydes: formaldehyde, acetaldehyde, hydroxyacetaldehyde, glyoxal, methylglyoxal	10–20
Carboxylic acids: formic, acetic, propionic, butyric, pentanoic, hexanoic, glycolic, hydroxy acids	10–15
Carbohydrates: cellobiosan, α-D-levoglucosan, oligosaccharides, 1,6 anhydroglucofuranose	5–10
Phenols: phenol, cresol, guaiacol, syringyl	2–5
Furfurols	1–4
Alcohols: methanol, ethanol	2–5
Ketones: acetol (1-hydroxy-2-propanone), cyclopentanones	1–5

**Values taken from Barandas (2009).*

Yan et al. (2010), tested the hydrogen conversion of nickel catalysts supported on CeO_2-ZrO_2 and commercial nickel catalysts (Z417). The presence of a carrier with reducible oxides increased the percentage of hydrogen produced per gram of catalyst, promoted increased catalyst cycling, and increased the useful life of the catalyst. Zhang et al. (2012), reported similar results using bimetallic Ni and Co catalysts on CeO_2-ZrO_2 supports compared to Ni and Co catalysts. The interactions of the mixed oxides created catalytic sites for breaking CC and CH bonds and vacancy formation and reabsorption of oxygen molecules assisted in the removal of carbon deposits formed on the catalyst surface.

Hydrogen Production via the Gas-Water Displacement Reaction (Water Gas Shift)

The gas-water displacement reaction (WGS) is important because it decreases CO concentration and produces hydrogen (the desired product) concomitantly. Even in small amounts, CO exhaust gas must be removed due to its adverse effects on the anodes of fuel cells, causing the deactivation of electrocatalysts (Ghenciu, 2002).

$$CO(g) + H_2O(\text{steam}) CO_2(g) + H_2(g) (\text{WGS reaction})$$

Although relatively simple (compared to bio-oil reactions), WGS requires high selectivity and high yield. Recombination reaction between CO and CO_2 molecules for the formation of short chain oxygenates should also be suppressed. The formation of carbonaceous molecules on the surface of the catalysts can result in carbon deposits and consequent passivation of the catalyst. Two characteristics of reducible oxides highlight their applicability for this reaction: (i) abundant vacancies and (ii) interactions with oxygen (Zhai et al., 2010). The creation of

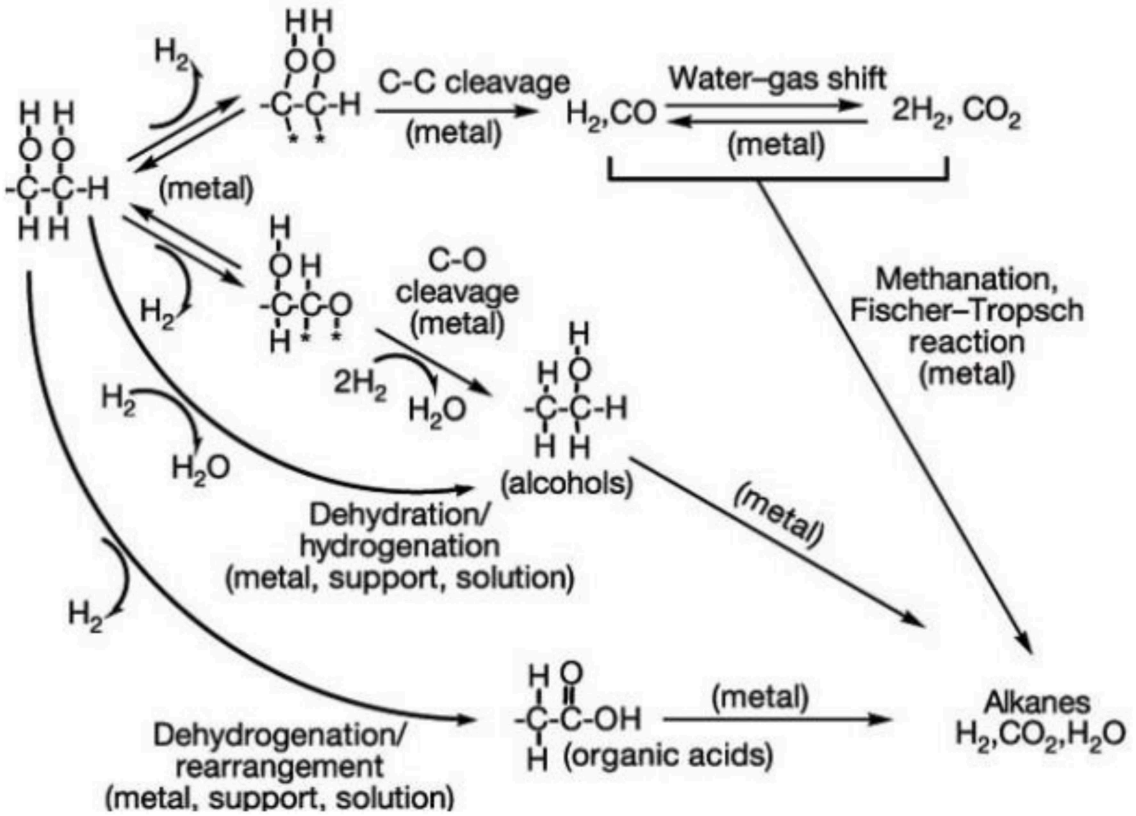

FIGURE 12 | Reaction paths for hydrogen production from compounds (adapted from Cortright et al., 2002).

electropositive sites (vacancies) increases the spill over of water molecules and creation of highly reactive radicals (OH and OOH). The liberation and adsorption of oxygen is another key to the excellent performance of catalysts based on reducible oxides, since they can remove O in H_2O and react with CO to form CO_2 and H_2 (Pazmiño et al., 2012). In addition, reducible oxides form peroxo species that are very reactive on the surface, minimizing carbon deposit formation. These oxides also exhibit high oxygen mobility on the surface, increasing the reaction dynamics between the peroxo species and carbon deposits, leaving the catalysts (hot spot zones) available for reaction. In general, the higher reactivity of the reducible oxides is linked to the formed vacancies. Vindigni et al. (2012), observed improved dispersion and smaller gold nanoparticles with the addition of ZrO_2 to CeO_2-containing supports. While the vacancies and their interaction with the nanoparticles effectively prevented agglomeration. With improved nanoparticle dispersion and abundant vacancies, a greater the number of reaction sites become available, resulting in greater activity. In this same study, it was verified that upon addition of ZrO_2 to CeO_2, a considerable increase in the acidity of the support occurred, which is unfavorable for some reactions (Vindigni et al., 2012). Even with the increased number of vacancies and increased dispersion of the supported metal, the interaction between the reactants and catalyst can be hampered by increased electrostatic repulsion. To avoid these problems, many researchers have focused on the addition of basic promoters (usually groups I and II atoms) to increase support basicity and spill over (Zhai et al., 2010; Pazmiño et al., 2012).

Production of Hydrogen From the Preferential Oxidation of CO (Prox)

The conventional method of producing hydrogen combines reactions of bio-oil reforming with the WGS, which generates gases with the following composition: 45% H_2, 25% CO_2, 10% H_2O, 20% N_2, and 0.5–1% CO. At low concentrations (0.5–1%), CO negatively impacts the performance of the fuel cell electrocatalysts. Thus, CO removal, i.e., reducing its concentration to < 10 ppm, can be achieved by preferential oxidation of CO (Prox). Wootsch et al. (2004) compared the performance of Pt nanoparticles supported on Al_2O_3 with the same nanoparticles supported on CeO_2-ZrO_2 for the Prox reaction. CeO_2-ZrO_2 was more active at low temperatures due to its non-competitive reaction mechanism, where the H_2 and CO molecules do not react at the catalytic sites. The H_2 molecules react in the vicinity of the nanoparticles due to the interaction of the noble metal with H_2, whereas the addition of oxygen to CO occurs preferentially at the vacancy sites. However, the use of reducible oxides for the Prox reaction at high temperatures is not efficient compared to other oxide catalysts because with

increasing temperature, many vacancies are formed and the oxidation of H_2 becomes favorable. This results in a reduction of CO oxidation activity, while consuming the H_2 formed in the other steps (Wootsch et al., 2004). Sangeetha and Chen (2009), added CeO_2 and CoO to catalysts containing Au nanoparticles supported on TiO_2. With the addition of these mixed oxides to the catalyst, the activity and selectivity of the Prox reaction were improved.

ELECTROCATALYTIC REACTIONS FROM OXIDE

Hence, fundamentally, an electrocatalyst can be usually defined as a complex material which interacts with some certain species, without being consumed during an electrochemical target reaction (Seh et al., 2017). Some examples of reducible oxides applied as electrocatalyst will be discussed below.

Production of Solid Carbon Species From CO_2

A recent study shows an interaction between CO_2, in its gaseous state, with a thin 2D layer of ceria nanoparticles formed on a metal/electrolyte interface, providing a faradaic efficiency of ∼75% (Esrafilzadeh et al., 2019). The electrocatalysis reaction occurs from this interaction and produces solid carbonaceous species, at ordinary room temperature and low voltage (−310 mV) (Esrafilzadeh et al., 2019). This process of reversing combustion over a liquid catalyst has a great advantage over solid catalysts. Since the latter is easily deactivated by the formation of surface coke, the former becomes an alternative of great technological interest and can be produced on a large scale for application in negative CO_2 emission technology (Taccardi et al., 2017; Esrafilzadeh et al., 2019). However, (Esrafilzadeh et al., 2019) experimented with the variation in potential applied in electrocatalysis and also produces CO as one of the products. Between the potential range of −3 to −2.5 V vs. Ag/Ag^+ showed higher CO production while −1.8 to −2.0 V vs. Ag/Ag^+ there was a higher production of carbonaceous materials. The potential range, therefore, thus showed the selectivity of the products (Esrafilzadeh et al., 2019).

Reduction of N_2 to NH_3

The electrochemical N_2 reduction reaction (NRR), under ambient conditions for formation of NH_3, performed with CeO_2 nanorods with oxygen vacancies by Xu et al., had a performance of 16.4 $\mu g\, h^{-1} mg_{cat}^{-1}$ at −0.5 V vs. reversible hydrogen electrode (RHE) and Faradaic efficiency of 3.7% at −0.4 V vs. RHE using 0.1 M aqueous Na_2SO_4 electrolyte (Xu et al., 2019). On the other hand, the pristine CeO_2 presented performance of 5.4 $\mu g h^{-1} mg_{cat}^{-1}$ and 2.1%, respectively. The oxygen vacancies induced by the heat treatment, with a current of H_2 inside a tube furnace, played a key role in the crystalline network CeO_2 optimizing production by 2.8 times. This technology allows the innovation of artificial N_2 fixation, having great importance in the production of fertilizers, medicines and combustion fuel, for example (Christensen et al., 2006; Erisman et al., 2008; Service, 2014; Xu et al., 2019).

CONCLUDING REMARKS AND PERSPECTIVES

In summary, reducible oxides are materials that have the capacity to undergo changes in oxidation state by the output of an oxygen atom from the oxide network. Overall, vacancy formation is favored at higher temperatures and lower partial pressures of O_2. Upon addition of dopants, the structure promotes the reduction of the oxides through destabilization of the crystalline lattice and donation of electronic density to the energy gap. In this manner, the use of reducible oxides can increase the catalytic activity resulting from increased interaction between the dopant and oxide. The use of mixed reducible oxides (CeO_2 + ZrO_2) or more complex oxides (such as $BaTiO_3$, $LaCoO_3$, and $HfSiO_X$) stabilize the vacancies and provide thermal and physical stability to the reducible oxide systems. However, the role played by both phases of the oxide and a generally accepted mechanism for the oxidation reaction remains unknown. Hence, vacancy-like formation is essential for the catalyst performance of a huge variety of reducible oxides. Many reactions naturally depend on the metal vacancy interface for bond cleavage and desired product formation. Therefore, the use of reducible oxides for the production of hydrogen is advantageous, as it increases the cycling number of the catalyst, reduces carbon deposition, and increases the conversion and selectivity of the reactions. Despite many advances, the theoretical and experimental study of materials based on reducible oxides remains in its infancy, as many important issues remain regarding these systems. Theoretical methods require precise prediction of the multielectron orbital energies at different oxidation states. In addition to theoretical advancement, a greater amount of data is required to understand the nature and role of defects in the reactivity of catalysts based on reductive oxides. The use of reducible oxides on a large scale has not yet been achieved because of the high price of these materials compared to other commonly used oxides. Therefore, comparing the market prices for silicon and aluminum oxides (which are abundant and easily exploited) with those of reducible oxides (which are less abundant and often require removal from other minerals), it is clear that the production and improvement of its applications are necessary to achieve a positive cost/benefit ratio.

AUTHOR CONTRIBUTIONS

FL designed the study and contributed to the review of the whole manuscript. FP wrote most of the manuscript with help from VS and RS. All authors discussed the results and contributed to the final manuscript.

ACKNOWLEDGMENTS

The authors thank to the financial support of the CNPq, CAPES, Fundação Araucária and FAPEMIG.

REFERENCES

Aranda, A., Agouram, S., López, J. M., Mastral, A. M., Sellick, D. R., Solsona, B., et al. (2012). Oxygen defects: the key parameter controlling the activity and selectivity of mesoporous copper-doped ceria for the total oxidation of naphthalene. *Appl. Catal. B Environ.* 127, 77–88. doi: 10.1016/j.apcatb.2012.07.033

Araújo, V. D., Avansi, W., De Carvalho, H. B., Moreira, M. L., Longo, E., Ribeiro, C., et al. (2012). CeO_2 nanoparticles synthesized by a microwave-assisted hydrothermal method: evolution from nanospheres to nanorods. *CrystEngComm* 14, 1150–1154. doi: 10.1039/C1CE06188G

Aškrabiać, S., Dohčeviać-Mitroviać, Z., Kremenoviać, A., Lazareviać, N., Kahlenberg, V., and Popoviać, Z. V. (2012). Oxygen vacancy-induced microstructural changes of annealed CeO_2-x nanocrystals. *J. Raman Spectrosc.* 43, 76–81. doi: 10.1002/jrs.2987

Ávila-neto, C. N., Liberatori, J. W. C., Silva, A. M., Zanchet, D., Hori, C. E., Noronha, F. B., et al. (2012). Understanding the stability of Co-supported catalysts during ethanol reforming as addressed by *in situ* temperature and spatial resolved XAFS analysis. *J. Catal.* 287, 124–137. doi: 10.1016/j.jcat.2011.12.013

Barandas, A. P., Passos, M. G., and Noronha, F. B. (2011) "Estudo do mecanismo da reação de produção de hidrogênio a partir da reforma oxidativa do acetol utilizando catalisadores de Ni/γ-Al_2O_3," in *16o Congresso Brasileiro de Catálise*, (Campos do Jordão), 678–683.

Barandas, A. P. M. G. (2009). *Produção de Hidrogênio a Partir do Acetol Em Catalisadores de Níquel Suportados Produção de Hidrogênio a Partir do Acetol em Catalisadores de Níquel Suportados* ANA PAULA MAURO GONÇALVES BARANDAS.

Barcaro, G., and Fortunelli, A. (2019). 2D oxides on metal materials: concepts, status, and perspectives. *Phys. Chem. Chem. Phys.* 21, 11510–11536. doi: 10.1039/C9CP00972H

Basagiannis, A. C., and Verykios, X. E. (2006). Reforming reactions of acetic acid on nickel catalysts over a wide temperature range. *Appl. Catal. A Gen.* 308, 182–193. doi: 10.1016/j.apcata.2006.04.024

Basagiannis, A. C., and Verykios, X. E. (2007). Catalytic steam reforming of acetic acid for hydrogen production. *Int. J. Hydrogen Energy* 32, 3343–3355. doi: 10.1016/j.ijhydene.2007.04.039

Brenner, T. M., Egger, D. A., Kronik, L., Hodes, G., and Cahen, D. (2016). Hybrid organic—inorganic perovskites: low-cost semiconductors with intriguing charge-transport properties. *Nat. Rev. Mater.* 1:15007. doi: 10.1038/natrevmats.2015.7

Bryant, B., Renner, C. H., Tokunaga, Y., Tokura, Y., and Aeppli, G. (2011). Imaging oxygen defects and their motion at a manganite surface. *Nat. Commun.* 2, 212–216. doi: 10.1038/ncomms1219

Callister, W. D., and Rethwisch, D. (2012). *Fundamentals of Materials Science and Engineering: An Integrated Approach.* Hoboken, NJ: John Wiley & Sons.

Campbell, C. T. (2003). Surface science. Waltzing with O_2. *Science* 299:357. doi: 10.1126/science.1081090

Capdevila-Cortada, M., and López, N. (2017). Entropic contributions enhance polarity compensation for CeO_2 (100) surfaces. *Nat. Mater.* 16, 328–334. doi: 10.1038/nmat4804

Christensen, C. H., Johannessen, T., Sørensen, R. Z., and Nørskov, J. K. (2006). Towards an ammonia-mediated hydrogen economy? *Catal. Today* 111, 140–144. doi: 10.1016/j.cattod.2005.10.011

Cortright, R. D., Davda, R. R., and Dumesic, J. A. (2002). Hydrogen from catalytic reforming of biomass-derived hydrocarbons in liquid water. *Nature* 418, 964–967. doi: 10.1038/nature01009

da Fonseca, A. F. V., Siqueira, R. L., Landers, R., Ferrari, J. L., Marana, N. L., Sambrano, J. R., et al. (2018). A theoretical and experimental investigation of Eu-doped ZnO nanorods and its application on dye sensitized solar cells. *J. Alloys Compd.* 739, 939–947. doi: 10.1016/j.jallcom.2017.12.262

de Castro, I. A., Datta, R. S., Ou, J. Z., Castellanos-Gomez, A., Sriram, S., Daeneke, T., et al. (2017). Molybdenum oxides – from fundamentals to functionality. *Adv. Mater.* 29, 1–31. doi: 10.1002/adma.201701619

de Lasa, H., Salaices, E., Mazumder, J., and Lucky, R. (2011). Catalytic steam gasification of biomass: catalysts, thermodynamics and kinetics. *Chem. Rev.* 111, 5404–5433. doi: 10.1021/cr200024w

Dubey, V. R., and Vaidya, P. D. (2012). Kinetics of steam reforming of acetol over a Pt/C catalyst. *Chem. Eng. J.* 180, 263–269. doi: 10.1016/j.cej.2011.11.034

Erisman, J. W., Sutton, M. A., Galloway, J., Klimont, Z., and Winiwarter, W. (2008). How a century of ammonia synthesis changed the world. *Nat. Geosci.* 1, 636–639. doi: 10.1038/ngeo325

Esch, F., Fabris, S., Zhou, L., Montini, T., Africh, C., Fornasiero, P., et al. (2005). Electron localization determines defect formation on ceria substrates. *Science* 309, 752–755. doi: 10.1126/science.1111568

Esrafilzadeh, D., Zavabeti, A., Jalili, R., Atkin, P., Choi, J., Carey, B. J., et al. (2019). Room temperature CO_2 reduction to solid carbon species on liquid metals featuring atomically thin ceria interfaces. *Nat. Commun.* 10:865. doi: 10.1038/s41467-019-09228-4

Feng, B., Sugiyama, I., Hojo, H., Ohta, H., Shibata, N., and Ikuhara, Y. (2016). Atomic structures and oxygen dynamics of CeO_2 grain boundaries. *Sci. Rep.* 6, 1–7. doi: 10.1038/srep20288

Fernandes, S. L., Albano, L. G. S., Affonço, L. J., da Silva, J. H. D., Longo, E., Graeff, C. F. O. (2019). Exploring the properties of niobium oxide films for electron transport layers in perovskite solar cells. *Front. Chem.* 7:50. doi: 10.3389/fchem.2019.00050

Ghenciu, A. F. (2002). Review of fuel processing catalysts for hydrogen production in PEM fuel cell systems. *Curr. Opin. Solid State Mater. Sci.* 6, 389–399. doi: 10.1016/S1359-0286(02)00108-0

Glunz, S. W., Preu, R., and Biro, D. (2012). "Crystalline silicon solar cells: state-of-the-art and future developments," in *Comprehensive Renewable Energy 1: Photovoltaic Solar Energy (Technology)* (Elsevier), 353–387.

Gong, J., Sumathy, K., Qiao, Q., and Zhou, Z. (2017). Review on dye-sensitized solar cells (DSSCs): advanced techniques and research trends. *Renew. Sustain. Energy Rev.* 68, 234–246. doi: 10.1016/j.rser.2016.09.097

Grover, V., Banerji, A., Sengupta, P., and Tyagi, A. K. (2008). Raman, XRD and microscopic investigations on CeO_2-Lu_2O_3 and CeO_2-Sc_2O_3 systems: a sub-solidus phase evolution study. *J. Solid State Chem.* 181, 1930–1935. doi: 10.1016/j.jssc.2008.04.001

Guo, X., and Waser, R. (2006). Electrical properties of the grain boundaries of oxygen ion conductors: acceptor-doped zirconia and ceria. *Prog. Mater. Sci.* 51, 151–210. doi: 10.1016/j.pmatsci.2005.07.001

Hardacre, C., Roe, G. M., and Lambert, R. M. (1995). Structure, composition and thermal properties of cerium oxide films on platinum {111}. *Surf. Sci.* 326, 1–10. doi: 10.1016/0039-6028(94)00783-7

Holladay, J. D., Hu, J., King, D. L., and Wang, Y. (2009). An overview of hydrogen production technologies. *Catal. Today* 139, 244–260. doi: 10.1016/j.cattod.2008.08.039

Jiang, D., Wang, W., Zhang, L., Zheng, Y., and Wang, Z. (2015). Insights into the surface-defect dependence of photoreactivity over CeO_2 nanocrystals with well-defined crystal facets. *ACS Catal.* 5, 4851–4858. doi: 10.1021/acscatal.5b01128

Kripal, R., Gupta, A. K., Srivastava, R. K., and Mishra, S. K. (2011). Photoconductivity and photoluminescence of ZnO nanoparticles synthesized via co-precipitation method. *Spectrochim. Acta Part A Mol. Biomol. Spectrosc.* 79, 1605–1612. doi: 10.1016/j.saa.2011.05.019

Łamacz, A., Krztoń, A., and Djéga-Mariadassou, G. (2011). Steam reforming of model gasification tars compounds on nickel based ceria-zirconia catalysts. *Cataly. Today.* 176, 347–351. doi: 10.1016/j.cattod.2010.11.067

Lee, W., Jung, H. J., Lee, M. H., Kim, Y. B., Park, J. S., Sinclair, R., et al. (2012). Oxygen surface exchange at grain boundaries of oxide ion conductors. *Adv. Funct. Mater.* 22, 965–971. doi: 10.1002/adfm.201101996

Li, C., Li, X., Liu, L., Wang, H., and Yang, W. (2018). Synthesis of novel 2D ceria nanoflakes with enhanced catalytic activity induced by cobalt doping. *Mater. Lett.* 230, 80–83. doi: 10.1016/j.matlet.2018.07.030

Liu, B., Liu, B., Li, Q., Du, X., Yao, M., Li, Z., et al. (2011). Facile hydrothermal synthesis of CeO_2 nanosheets with high reactive exposure surface. *J. Alloys Compd.* 509, 6720–6724. doi: 10.1016/j.jallcom.2011.03.156

Liu, D., Lv, Y., Zhang, M., Liu, Y., Zhu, Y., Zong, R., et al. (2014). Defect-related photoluminescence and photocatalytic properties of porous ZnO nanosheets. *J. Mater. Chem. A* 2, 15377–15388. doi: 10.1039/C4TA02678K

Livage, J. (2010). Hydrothermal synthesis of nanostructured vanadium oxides. *Materials.* 3, 4175–4195. doi: 10.3390/ma3084175

Lu, X. H., Huang, X., Xie, S. L., Zheng, D. Z., Liu, Z. Q., Liang, C. L., et al. (2010). Facile electrochemical synthesis of single crystalline CeO_2 octahedrons and their optical properties. *Langmuir* 26, 7569–7573. doi: 10.1021/la904882t

Manser, J. S., Christians, J. A., and Kamat, P. V. (2016). Intriguing optoelectronic properties of metal halide perovskites. *Chem. Rev.* 116, 12956–13008. doi: 10.1021/acs.chemrev.6b00136

Masi, S., Mastria, R., Scarfiello, R., Carallo, S., Nobile, C., Gambino, S., et al. (2018). Room-temperature processed films of colloidal carved rod-shaped nanocrystals of reduced tungsten oxide as interlayers for perovskite solar cells. *Phys. Chem. Chem. Phys.* 20, 11396–11404. doi: 10.1039/C8CP00645H

Migani, A., Vayssilov, G. N., Bromley, S. T., Illas, F., and Neyman, K. M. (2010). Greatly facilitated oxygen vacancy formation in ceria nanocrystallites. *Chem. Commun.* 46, 5936–5938. doi: 10.1039/c0cc01091j

Misono, M. (2005). A view on the future of mixed oxide catalysts. *Catal. Today* 100, 95–100. doi: 10.1016/j.cattod.2004.12.010

Montini, T., Speghini, A., De Rogatis, L., Lorenzut, B., Bettinelli, M., Graziani, M., et al. (2009). Identification of the structural phases of Ce(x)Zr(1-x)O2 by Eu(III) luminescence studies. *J Am Chem Soc.* 131, 13155–13160. doi: 10.1021/ja905158p

Mora-Fonz, D., Lazauskas, T., Farrow, M. R., Catlow, C. R. A., Woodley, S. M., and Sokol, A. A. (2017). Why are polar surfaces of ZnO stable? *Chem. Mater.* 29, 5306–5320. doi: 10.1021/acs.chemmater.7b01487

Morris, M. C., McMurdie, H. F., Evans, E. H., Paretzkin, B., Parker, H. S., et al. (1964). *Standard X-Ray Diffraction Powder Patterns. Monograph* 25 *Section 20*. Washington, DC: Government Printing Office.

Namai, Y., Fukui, K., and Iwasawa, Y. (2003b). Atom-resolved noncontact atomic force microscopic observations of CeO_2 (111) surfaces with different oxidation states: surface structure and behavior of surface oxygen atoms. *J. Phys. Chem. B* 107, 11666–11673. doi: 10.1021/jp030142q

Namai, Y., Fukui, K.-I., and Iwasawa, Y. (2003a). Atom-resolved noncontact atomic force microscopic and scanning tunneling microscopic observations of the structure and dynamic behavior of CeO_2(111) surfaces. *Catal. Today* 85, 79–91. doi: 10.1016/S0920-5861(03)00377-8

National Renewable Energy Laboratory (2019). Available online at: https://www.nrel.gov/pv/cell-efficiency.html

Nolan, M., Fearon, J. E., and Watson, G. W. (2006). Oxygen vacancy formation and migration in ceria. *Solid State Ionics* 177, 3069–3074. doi: 10.1016/j.ssi.2006.07.045

Nunes, D., Pimentel, A., Santos, L., Barquinha, P., Pereira, L., Fortunato, E., et al. (Eds.). (2018). "6 – Oxide materials for energy applications," in *Metal Oxide Nanostructures* (Elsevier), 199–234. doi: 10.1016/B978-0-12-811512-1.00006-0

O'Regan, B., and Gratzel, M. (1991). A low-cost, high-efficiency solar cell based on dye-sensitized colloidal TiO2 films. *Nature* 353, 737–740. doi: 10.1038/353737a0

Paier, J., Penschke, C., and Sauer, J. (2013). Oxygen defects and surface chemistry of ceria: quantum chemical studies compared to experiment. *Chem. Rev.* 113, 3949–3985. doi: 10.1002/chin.201333211

Pazmiño, J. H., Shekhar, M., Damion Williams, W., Cem Akatay, M., Miller, J. T., Nicholas Delgass, W., et al. (2012). Metallic Pt as active sites for the water–gas shift reaction on alkali-promoted supported catalysts. *J. Catal.* 286, 279–286. doi: 10.1016/j.jcat.2011.11.017

Polman, A., Knight, M., Garnett, E. C., Ehrler, B., and Sinke, W. C. (2016). Photovoltaic materials – present efficiencies and future challenges. *Science* 352:aad4424. doi: 10.1126/science.aad4424

Protesescu, L., Yakunin, S., Bodnarchuk, M. I., Krieg, F., Caputo, R., Hendon, C. H., et al. (2015). Nanocrystals of cesium lead halide perovskites (CsPbX3, X = Cl, Br, and I): novel optoelectronic materials showing bright emission with wide color gamut. *Nano Lett.* 15, 3692–3696. doi: 10.1021/nl5048779

Ramirez, D., Velilla, E., Montoya, J. F., and Jaramillo, F. (2019). Mitigating scalability issues of perovskite photovoltaic technology through a p-i-n meso-superstructured solar cell architecture. *Solar Energy Mater. Solar Cells* 195, 191–197. doi: 10.1016/j.solmat.2019.03.014

Rasmussen, M. D., Molina, L. M., and Hammer, B. (2004). Adsorption, diffusion, and dissociation of molecular oxygen at defected TiO2(110): a density functional theory study. *J. Chem. Phys.* 120, 988–997. doi: 10.1063/1.1631922

Rodriguez, J. A., Graciani, J., Evans, J., Park, J. B., Yang, F., Stacchiola, D., et al. (2009). Water-gas shift reaction on a highly active inverse CeO, x/Cu(111) catalyst: unique role of ceria nanoparticles. *Angew. Chem. Int. Ed.* 48, 8047–8050. doi: 10.1002/anie.200903918

Rodríguez, J. A., and Hrbek, J. (2010). Surface science inverse oxide/metal catalysts : a versatile approach for activity tests and mechanistic studies. *Surf. Sci.* 604, 241–244. doi: 10.1016/j.susc.2009.11.038

Saliba, M., Matsui, T., Domanski, K., Correa-Baena, J.-P., Nazeeruddin, M. K., Zakeeruddin, S. M., et al. (2016). Cesium-containing triple cation perovskite solar cells: improved stability, reproducibility and high efficiency. *Energy Environ. Sci.* 9, 1989–1997. doi: 10.1039/C5EE03874J

Sangeetha, P., and Chen, Y.-W. (2009). Preferential oxidation of CO in H2 stream on Au/CeO_2–TiO2 catalysts. *Int. J. Hydrogen Energy* 34, 7342–7347. doi: 10.1016/j.ijhydene.2009.06.045

Schaub, R., Wahlström, E., Rønnau, A., Lægsgaard, E., Stensgaard, I., and Besenbacher, F. (2003). Oxygen-mediated diffusion of oxygen vacancies on the TiO2(110) surface. *Science* 299, 377–379. doi: 10.1126/science.1078962

Seh, Z. W., Kibsgaard, J., Dickens, C. F., Chorkendorff, I. B., Nørskov, J. K., and Jaramillo, T. F. (2017). Combining theory and experiment in electrocatalysis: insights into materials design. *Science* 355:eaad4998. doi: 10.1126/science.aad4998

Service, R. F. (2014). New recipe produces ammonia from air, water, and sunlight. *Science* 345:610. doi: 10.1126/science.345.6197.610

Sharma, S., Siwach, B., Ghoshal, S. K., and Mohan, D. (2017). Dye sensitized solar cells: from genesis to recent drifts. *Renew. Sustain. Energy Rev.* 70, 529–537. doi: 10.1016/j.rser.2016.11.136

Song, C., Zhao, J., Li, H., Luo, S., Tang, Y., and Wang, D. (2017). Design, controlled synthesis, and properties of 2D CeO_2/NiO heterostructure assemblies. *CrystEngComm* 19, 7339–7346. doi: 10.1039/C7CE01769C

Song, H., Mirkelamoglu, B., and Ozkan, U. S. (2010). Effect of cobalt precursor on the performance of ceria-supported cobalt catalysts for ethanol steam reforming. *Appl. Catal. A Gen.* 382, 58–64. doi: 10.1016/j.apcata.2010.04.016

Soykal, I. I., Bayram, B., Sohn, H., Gawade, P., Miller, J. T., and Ozkan, U. S. (2012). Ethanol steam reforming over Co/CeO_2 catalysts: investigation of the effect of ceria morphology. *Appl. Catal. A Gen.* 449, 47–58. doi: 10.1016/j.apcata.2012.09.038

Sun, C., Li, H., and Chen, L. (2012). Nanostructured ceria-based materials: synthesis, properties, and applications. *Energy Environ. Sci.* 5, 8475–8505. doi: 10.1039/c2ee22310d

Swartz, S. L. (2002). "Catalysis by ceria and related materials Edited by Alessandro Trovarelli (Università di Udine, Italy). catalytic science series. volume 2. Series Edited by Graham J. Hutchings. Imperial College Press: London. 2002. vviii + 508 pp. $78.00. ISBN: 1-86094-29. *J. Am. Chem. Soc.* 124, 12923–12924. doi: 10.1021/ja025256e

Taccardi, N., Grabau, M., Debuschewitz, J., Distaso, M., Brandl, M., Hock, R., et al. (2017). Gallium-rich Pd-Ga phases as supported liquid metal catalysts. *Nat. Chem.* 9, 862–867. doi: 10.1038/nchem.2822

Tiseanu, C., Parvulescu, V., Avram, D., Cojocaru, B., Boutonnet, M., and Sanchez-Dominguez, M. (2014). Local structure and nanoscale homogeneity of CeO_2-ZrO_2: differences and similarities to parent oxides revealed by luminescence with temporal and spectral resolution. *Phys. Chem. Chem. Phys.* 16, 703–710. doi: 10.1039/C3CP52893F

Trane, R., Dahl, S., Skjøth-Rasmussen, M. S., and Jensen, A. D. (2012). Catalytic steam reforming of bio-oil. *Int. J. Hydrogen Energy* 37, 6447–6472. doi: 10.1016/j.ijhydene.2012.01.023

Trovarelli, A., and Fornasiero, P. (eds.). (2013). *Catalysis by Ceria and Related Materials*. Vol. 12. World Scientific. doi: 10.1142/p870

Umar, A., Kumar, R., Akhtar, M. S., Kumar, G., and Kim, S. H. (2015). Growth and properties of well-crystalline cerium oxide (CeO_2) nanoflakes for environmental and sensor applications. *J. Colloid Interface Sci.* 454, 61–68. doi: 10.1016/j.jcis.2015.04.055

Vagia, E. C., and Lemonidou, A. A. (2008). Thermodynamic analysis of hydrogen production via autothermal steam reforming of selected components of aqueous bio-oil fraction. *Int. J. Hydrogen Energy* 33, 2489–2500. doi: 10.1016/j.ijhydene.2008.02.057

Van Santen, R. A., Tranca, I., and Hensen, E. J. M. (2015). Theory of surface chemistry and reactivity of reducible oxides. *Catal. Today* 244, 63–84. doi: 10.1016/j.cattod.2014.07.009

Vayssilov, G. N., Lykhach, Y., Migani, A., Staudt, T., Petrova, G. P., Tsud, N., et al. (2011). Support nanostructure boosts oxygen transfer to catalytically active platinum nanoparticles. *Nat. Mater.* 10, 310–315. doi: 10.1038/nmat2976

Velilla, E., Ramirez, D., Uribe, J.-I., Montoya, J. F., and Jaramillo, F. (2019). Outdoor performance of perovskite solar technology: silicon comparison and competitive advantages at different irradiances. *Solar Energy Mater. Solar Cells* 191, 15–20. doi: 10.1016/j.solmat.2018.10.018

Vindigni, F., Manzoli, M., Tabakova, T., Idakiev, V., Boccuzzi, F., and Chiorino, A. (2012). Gold catalysts for low temperature water-gas shift reaction: effect of ZrO 2 addition to CeO_2 support. *Appl. Catal. B Environ.* 125, 507–515. doi: 10.1016/j.apcatb.2012.05.031

Wagnerová, D. M., and Lang, K. (2011). Photorelease of triplet and singlet oxygen from dioxygen complexes. *Coord. Chem. Rev.* 255, 2904–2911. doi: 10.1016/j.ccr.2011.06.017

Wahlstro, E., Rønnau, A., Vestergaard, M., Lægsgaard, E., Stensgaard, I., and Besenbacher, F. (2004). Electron transfer–induced dynamics of oxygen molecules on the TiO 2 (110) surface. *Science* 303, 511–513. doi: 10.1126/science.1093425

Wang, J., Yan, C., Magdassi, S., and Lee, P. S. (2013). Zn2GeO4 nanowires as efficient electron injection material for electroluminescent devices. *ACS Appl. Mater. Interfaces* 5, 6793–6796. doi: 10.1021/am401234a

Wang, Q., Ito, S., Gratzel, M., Fabregat-Santiago, F., Mora-Seró, I., Bisquert, J., et al. (2006). Characteristics of high efficiency dye-sensitized solar cells. *J. Phys. Chem. B* 110, 25210–25221. doi: 10.1021/jp064256o

Wootsch, A., Descorme, C., and Duprez, D. (2004). Preferential oxidation of carbon monoxide in the presence of hydrogen (PROX) over ceria-zirconia and alumina-supported Pt catalysts. *J. Catal.* 225, 259–266. doi: 10.1016/j.jcat.2004.04.017

Xu, B., Xia, L., Zhou, F., Zhao, R., Chen, H., Wang, T., et al. (2019). Enhancing electrocatalytic N_2 reduction to NH_3 by CeO_2 nanorod with oxygen vacancies. *ACS Sustain. Chem. Eng.* 7, 2889–2893. doi: 10.1021/acssuschemeng.8b05007

Yan, C. F., Cheng, F. F., and Hu, R. R. (2010). Hydrogen production from catalytic steam reforming of bio-oil aqueous fraction over Ni/CeO_2-ZrO2 catalysts. *Int. J. Hydrogen Energy* 35, 11693–11699. doi: 10.1016/j.ijhydene.2010.08.083

Zhai, Y., Pierre, D., Si, R., Deng, W., Ferrin, P., Nilekar, A. U., et al. (2010). Alkali-stabilized Pt-OHx species catalyze low-temperature water-gas shift reactions. *Science* 329, 1633–1636. doi: 10.1126/science.1192449

Zhang, Y., Li, W., Zhang, S., Xu, Q., and Yan, Y. (2012). Steam reforming of bio-oil for hydrogen production: effect of Ni-Co bimetallic catalysts. *Chem. Eng. Technol.* 35, 302–308. doi: 10.1002/ceat.201100301

Zheng, Y., Li, K., Wang, H., Wang, Y., Tian, D., Wei, Y., et al. (2016). Structure dependence and reaction mechanism of CO oxidation: a model study on macroporous CeO_2 and CeO_2-ZrO_2 catalysts. *J. Catal.* 344, 365–377. doi: 10.1016/j.jcat.2016.10.008

Zhou, G., Hanson, J., and Gorte, R. J. (2008). A thermodynamic investigation of the redox properties of ceria-titania mixed oxides. *Appl. Catal. A Gen.* 335, 153–158. doi: 10.1016/j.apcata.2007.11.011

Conflict of Interest: The authors declare that the research was conducted in the absence of any commercial or financial relationships that could be construed as a potential conflict of interest.